# Observation of Inertial Particle Motion in Laminar Flow in a Stirred Vessel

Nishioka, Nami
Alatengtuya
Kumagai, Norihisa
Horie, Takafumi
Ohmura, Naoto

Memoirs of the Graduate School of Engineering Kobe University
No. 1, pp. 48–51, 2009. doi:10.5047/gseku.e.2009.003

# Observation of Inertial Particle Motion in Laminar Flow in a Stirred Vessel

Nami NISHIOKA[1], Alatengtuya[2*], Norihisa KUMAGAI[2], Takafumi HORIE[2], Naoto OHMURA[2]

[1]*Graduate School of Science and Technology, Department of Chemical Science and Engineering*
[2]*Graduate School of Engineering, Department of Chemical Science and Engineering*

(Received September 28, 2009; Accepted January 14, 2010; Online published January 21, 2010)

*Keywords:* *Stirred Vessel, Laminar Flow, Particle Motion, Solid-Liquid Flow, Nonlinear Dynamics*

**Inertial particle motion in a stirred vessel with no baffle plate was observed experimentally and numerically at low Reynolds numbers. Several particles were captured on a torus orbit within one of the IMRs and kept traveling around the impeller. The particles captured in the IMRs enhance the exchange of material with the outside active mixing region. The primary and secondary circulation flow directions were defined $\phi$- and $\theta$-direction respectively. Initially, particle orbit obtained by Poincaré section shows that the particle motion covers the full surface of the torus orbit and the ratio of the period for one round of a particle in $\phi$-direction to that in $\theta$-direction, $P_\theta/P_\phi$, is irrational, while after a long time, the circular orbit on the Poincaré section converges on three discrete points and $P_\theta/P_\phi$ is rational. Numerical simulation revealed that even after a particle seemed to have almost settled on a final orbit, the diameter of secondary circulation was not constant. After a particle has been captured, the drag force frequently works on the surface of the particle since the particle always exists near the impeller.**

## 1. Introduction

Mixing is one of the most important unit operations in chemical and biochemical industries. Stirred vessels commercially available in a wide variety of sizes and impeller configurations are the most frequently used to homogenize different substances, to conduct chemical reactions and to enhance mass transfer between different phases. Owing to their versatility, stirred vessels can be operated under a wide range of conditions. Although turbulent flow is efficient for mixing, some situations require laminar mixing, e.g. for high viscosity fluids and shear-sensitive materials. Koiranen *et al.*[1)] proposed specific principles for effective mixing in laminar flow mixing regimes for highly viscous liquids or shear-sensitive materials. In the laminar flow mixing regimes, however, global mixing is inefficient due to the existence of isolated mixing regions (IMRs). Much attention has been paid to how to eliminate IMRs at low Reynolds numbers. Lamberto *et al.*[2)] and Yao *et al.*[3)] demonstrated that IMRs could be eliminated by using an unsteady rotation method.

The authors[4)] found that particles released at the liquid surface were captured by the recirculation of IMRs. This phenomenon may conceivably affect laminar mixing characteristics in a stirred vessel. Furthermore, solid-liquid two-phase flows in stirred vessels are often encountered in industrial processes. The present work, therefore, observed inertial particle motion in a stirred vessel with no baffle plate experimentally and numerically at low Reynolds numbers.

## 2. Experiment and Numerical Simulation

In this study, inertial particle motion in a stirred vessel was investigated experimentally and numerically at low Reynolds numbers ($Re$ = 10, 30). The mixing system consists of a cylindrical flat-bottom vessel without baffle and a 4-bladed Rushton turbine, as shown in **Figure 1**. The origins of $r$- and $z$-coordinates are the center of the vessel shown in Figure 1 c). Detailed dimensions of the stirred vessel are shown in **Table 1**. The ratio of impeller off-bottom clearance to the tank diameter $C/T$ was 0.5. The working fluid was glycerine ($\rho$ = 1260 kg/m$^3$, $\mu$ = 1.4 Pa·s). In order to reduce photographic distortion, the cylindrical vessel was immersed

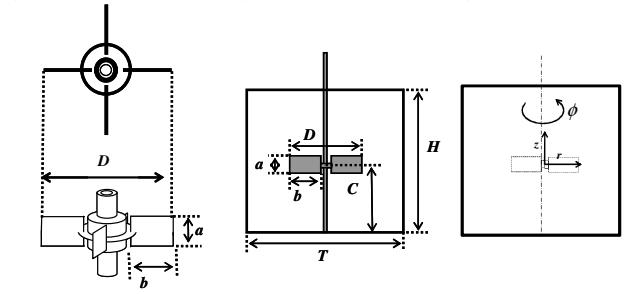


**Fig. 1** Schematic of stirred vessel: a) turbine impeller, b) stirred vessel and c) coordinate system

**Table 1** Dimensions of stirred vessel

| Symbols | [m] |
|---|---|
| $a$ | 0.02 |
| $b$ | 0.035 |
| $C$ | 0.1 |
| $D$ | 0.1 |
| $H$ | 0.2 |
| $T$ | 0.2 |

*Correspondence concerning this article should be addressed to Alatengtuya (E-mail: 078t4801t@stu.kobe-u.ac.jp).

into a square vessel of acrylic resin filled with the same glycerine.

Fluorescent pH-sensitive neutrally-buoyant green dye was used as a passive tracer to observe the mixing process. The working fluid was initially made basic by a small amount of basic solution consisting of 0.5 N NaOH and glycerine. After the turbine reached a certain rotational speed, a small amount of acidic solution consisting of 0.5 N HCl and glycerine was carefully added at the top of the vessel so as to decolorize the green dye by a neutralization reaction.The trajectories of resin particles having the density of 1377–1663 kg/m$^3$ and the diameter of 5 mm were analyzed using image processing. After a steady state was achieved, 10 particles were released on the upper surface at 1 or 5 cm away from the impeller axis.

The commercial CFD code RFLOW (Rflow Co, LTD) was used for the simulation of the motion of a particle. This numerical code is based on the finite volume method and makes it possible to simulate particle motion by a particle tracking method. All numerical conditions except particle size and particle density were the same as those for the experiment. The number of computational mesh is 60×60×60 in radial, circumferential and axial directions, respectively. Particle size and particle density were changed from $1.0\times10^{-6}$ to $1.0\times10^{-3}$ m and from 1200 to 1300 kg/m$^3$, respectively. Each particle was generated at the top of the device. At the first step, flow fields were obtained by solving the three-dimensional Navier-Stokes equations and the mass conservation for incompressible fluid in cylindrical coordinates. Then the particles were tracked by solving Eq. (1),

$$\rho_{\mathrm{p}}\frac{\mathrm{d}\mathbf{V}_{\mathrm{p}}}{\mathrm{d}t}=\frac{3}{4d_{\mathrm{p}}}C_{\mathrm{D}}\rho\left|\mathbf{V}-\mathbf{V}_{\mathrm{p}}\right|\left(\mathbf{V}-\mathbf{V}_{\mathrm{p}}\right) \qquad (1)$$
$$+\rho\frac{\mathrm{D}\mathbf{V}}{\mathrm{D}t}+\frac{1}{2}\rho\left(\frac{\mathrm{D}\mathbf{V}}{\mathrm{D}t}-\frac{\mathrm{D}\mathbf{V}_{\mathrm{p}}}{\mathrm{D}t}\right)+\left(\rho_{\mathrm{p}}-\rho\right)\mathbf{g}$$

where $\mathbf{V}_{\mathrm{p}}$ is the velocity of the particle, $\mathbf{V}$ is the velocity field of the fluid, $d_{\mathrm{p}}$ is the particle diameter, $\rho_{\mathrm{p}}$ is particle density, $\rho$ is fluid density, $\mathbf{g}$ is gravitational acceleration and $C_{\mathrm{D}}$ is the drag coefficient. The Basset history force, which is important in the initial motion of a particle starting from rest under certain conditions, was neglected.

## 3. Results and Discussion

As shown in **Figure 2**, when particles were released on the surface at 1.0 cm away from the impeller axis, several particles were captured on a torus orbit within the lower IMR and kept traveling around the impeller, while the rest of the particles sunk to the bottom of the vessel. On the other hand, when particles were released on the surface at 5.0 cm away from the impeller axis, several particles were captured on a torus orbit within the upper IMR (not shown in Figure 2). Initially, two IMRs clearly can be seen in Figure 2 a). After 18 h from the release of particle, the upper IMR having no particles is still visible, while the lower IMR having several particles is decolorized as shown in Figure 2b). This result indicates that particles captured in the IMRs enhance the exchange of material with the outside active mixing region. **Figure 3** shows the effect of particle motion on the exchange of material between the IMR and its surrounding AMR. When the particle approaches the outer layer of the IMR, the exchange of material between the IMR and AMR is enhanced. This result indicates that the particle orbits near the outer layer of the lower IMR play an important role in the elimination of IMR.

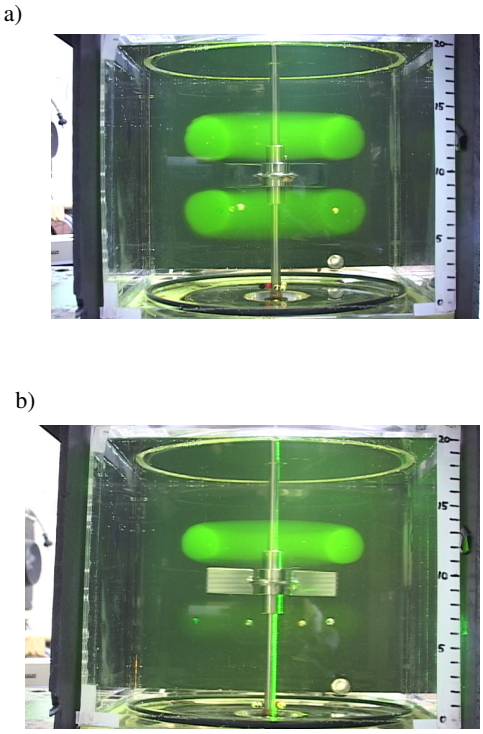


**Fig. 2** Flow visualization of IMRs in a stirred vessel: a) initial state and b) 18 h later ($Re$ = 10)

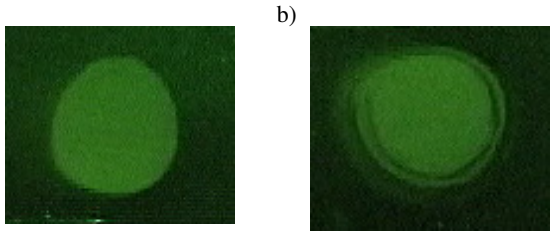


**Fig. 3** Effect of particle on the exchange of material between the IMR and its surrounding AMR: a) upper IMR and b) lower IMR

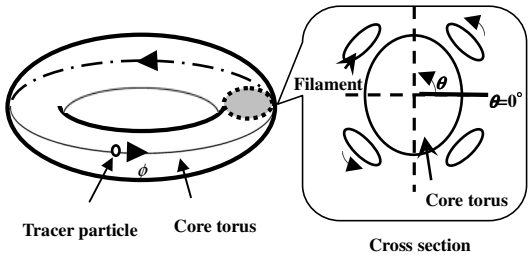


**Fig. 4** Schematic of Poincaré section corresponding to an arbitrary plane cutting a torus orbit transversally

In our previous works[4), 5)], the primary and secondary circulation flow directions were defined as $\phi$- and $\theta$-direction respectively and the period for one round of a particle in $\phi$-and $\theta$-direction is also defined as $P_\phi$ and $P_\theta$, as shown in **Figure 4**. This work also followed the above manner and investigated the relation between $P_\theta$ and $P_\phi$ of the particle

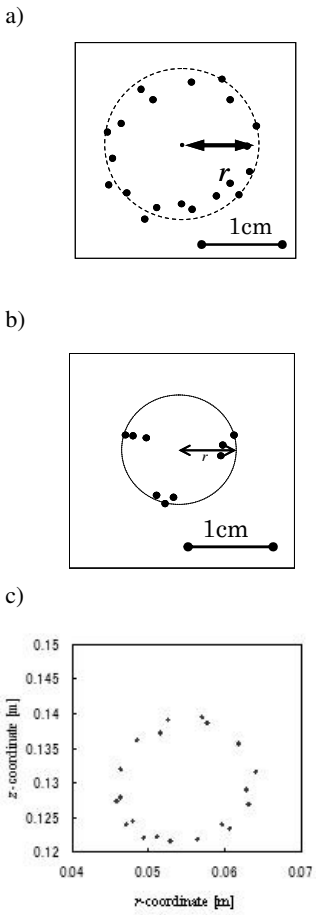


**Fig. 5** Poincaré sections of particle orbit at *Re*=10; a) experimental (1800 s), b) experimental (7200 s) and c) numerical (1800 s)

captured in the IMRs. In order to clarify particle orbit within IMR, this work constructed Poincaré sections corresponding to an arbitrary plane cutting a torus orbit transversally in the manner of nonlinear dynamics (see Figure 4). As shown in Figure 4, the return angle $\theta_n$ can be associated with the particle motion on the torus orbit. By selecting some arbitrary zero angle on the Poincaré section, the angle $\theta_n$ made by successive returns can be specified. A $\theta$-map (circle map) can be obtained by plotting the ($n$+1)th angle against nth. Particle orbit obtained by Poincaré section and $\theta$-map initially shows that the particle motion covers the full surface of the torus orbit and $P_\theta / P_\phi$ of the particle is irrational, as shown in **Figure 3 a)**. On the other hand, a circular orbit on the Poincaré section converges on three discrete points as shown in **Figure 3 b)**. This indicates that $P_\theta / P_\phi$ is rational and the particle motion becomes phase locked on the torus. Ohmura *et al.*[5] revealed that the ratio of the time period for one round of a filament around the core IMR in $\theta$-direction to the time for one round of a tracer particle in the filament in $\phi$-direction is rational. It can therefore be considered that particles initially move on the surface of the core torus and finally move in a filament within IMR. The particle trajectories obtained by numerical simulation show good agreement with the results of the experiment, as shown in **Figure 5 c)**. However, no phase-locked orbit could be observed in numerical simulations so far.

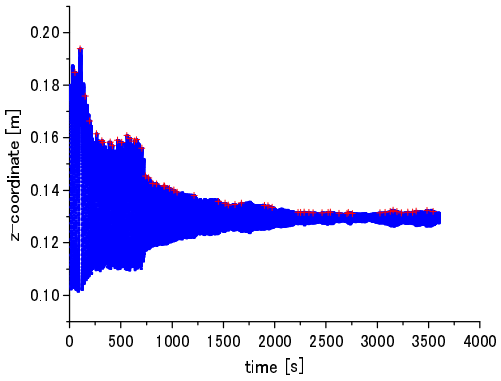


**Fig. 6** Numerically obtained time trace of particle position in z-component (*Re* = 10, $d_p$ = 8 mm, $\rho_p$ = 1200 kg/m$^3$)

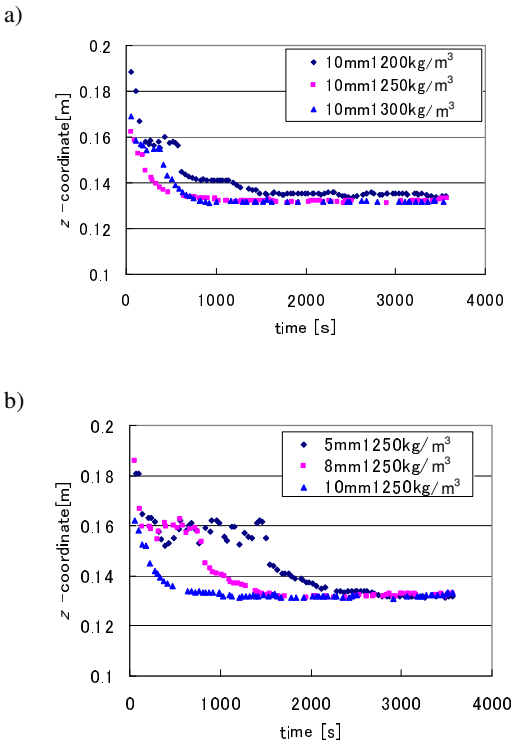


**Fig. 7** local maximum values of particle position in $z$-component against time (*Re*=10)

**Figure 6** shows numerically obtained time trace of particle position in $z$-component. This figure shows that the diameter of particle rotation orbit decreases stepwise with time. As can be seen during 250 and 750 s, even once a particle has settled on a certain orbit, the diameter fluctuates. Furthermore, even after a particle seems to have almost settled on a final orbit (after 2000 s), the diameter is not constant. This particle motion may contribute to enhancement of material exchange with the outside active mixing region, as previously shown in Figure 2 b). The effects of particle diameter and particle density on particle motions were investigated by extracting local maximum values of particle position in $z$-component.

As shown in **Figure7 a),** particles having the density larger than 1250 kg/m$^3$ converged at around 800 s, and they were faster than those having the density less than 1250 kg/m$^3$ when the particle diameter was 10 mm. The result for that of 8 mm showed the same tendency. However, no effect of the

particle density could be observed when the particle diameter was 5 mm. As for the effect of particle size, **Figure 7 b)** shows tendency that the larger particle is, the faster it converges.

### 4. Conclusions

In this study, inertial particle motion in a stirred vessel with no baffle plate was observed experimentally and numerically at low Reynolds numbers ($Re$ = 10). Several particles were captured on a torus orbit within one of the IMRs and kept traveling around the impeller. Which IMR particles are captured depends on the position of particles when released. Initially, particle orbit obtained by Poincaré section showed that the particle motion covered the full surface of the torus orbit and $P_\theta / P_\phi$ of the particle was irrational, while after a long time, the circular orbit on the Poincaré section converged on three discrete points. This indicates that $P_\theta / P_\phi$ is rational and the particle motion becomes phase-locked on the torus. Numerical simulation revealed that even after a particle seemed to have almost settled on a final orbit (after 2000 s), the diameter of secondary circulation was not constant. This particle motion may contribute to enhancement of material exchange with the outside active mixing region. After a particle has been captured, the drag force frequently works on the surface of the particle since the particle always exists near the impeller and the flow around the particle is repeatedly accelerated and decelerated by the impeller. This effect may enhance mass transfer between particle and liquid in IMRs.

#### Acknowledgements

This research was financially supported by a Grant-in-Aid for Scientific Research (A) (No. 20246115) from the Japan Society for the Promotion of Science (JSPS).

## Nomenclature

| | | | |
|---|---|---|---|
| $a$ | = | impeller blade height | [m] |
| $b$ | = | impeller blade width | [m] |
| $C$ | = | impeller off-bottom clearance | [m] |
| $C_D$ | = | drag force coefficient | [−] |
| $d_p$ | = | particle diameter | [m] |
| $D$ | = | impeller diameter | [m] |
| $H$ | = | height of tank | [m] |
| $N$ | = | rotational speed of impeller | [m] |
| $P_\phi$ | = | period for one round of a particle in $\phi$-direction | [s] |
| $P_\theta$ | = | period for one round of a particle in $\theta$-direction | [s] |
| $Re$ | = | Reynolds number (= $\rho ND^2/\mu$) | [m] |
| $T$ | = | tank diameter | [m] |
| $t$ | = | time | [s] |
| $\mathbf{V}$ | = | velocity vector of fluid | [m/s] |
| $\mathbf{V_P}$ | = | velocity vector of particle | [m/s] |
| $\mathbf{g}$ | = | gravitational acceleration | [m/s$^2$] |
| $\mu$ | = | viscosity | [Pa·s] |
| $\rho$ | = | fluid density | [kg/m$^3$] |
| $\rho_p$ | = | particle density | [kg/m$^3$] |

## Literature Cited

1) Koiranen, T., A. Kraslawski and L. Nyström; “Knowledge-based system for the preliminary design of mixing equipment,” *Ind. Eng. Chem. Res.*, **34**, 3059−3067 (1995)
2) Lamberto, D. J., F. J. Muzzio, P. D. Swanson and A. L. Tonkovich; “Using Time-Dependent RPM to Enhance Mixing in Stirred Vessels,” *Chem. Eng. Sci.*, **51**, 733−741 (1996)
3) Yao, W. G., H. Sato, K. Takahashi and K. Koyama; “Mixing Performance Experiments in Impeller Stirred Tanks Subjected to Unsteady Rotational Speeds,” *J. Chem. Eng. Japan*, **53**, 3031−3040 (1998)
4) Nishioka, N., Y. Tago, T. Takigawa, M. N. Noui-Mehidi, J. Wu and N. Ohmura; “Particle migration in a stirred vessel at low Reynolds numbers,” AIDIC Conference Series: Selected Papers of the Eighth Italian Conference on Chemical and Process Engineering, Vol. 8, pp. 243−247, Reed Business Information, Milano, Italy (2007)
5) Ohmura, N., T. Makino, T. Kaise, and K. Kataoka; “Transition of organized flow structure in a stirred vessel at low Reynolds numbers,” *J. Chem. Eng. Japan*, **36**, 1458−1463 (2003)